Free Radical Research, August 2010; 44(8): 936–949

Hoechst 33342 induces radiosensitization in malignant glioma cells via increase in mitochondrial reactive oxygen species

MOHAMMAD ATHAR[1], NABO K. CHAUDHURY[1], MOHAMMAD E. HUSSAIN[2] & RAJEEV VARSHNEY[1,3]

[1]*Division of Radiation Biosciences, Institute of Nuclear Medicine and Allied Sciences, Defence R&D Organization, Brig. S. K. Mazumdar Road, Delhi, India,* [2]*Department of Biosciences, Jamia Millia Islamia, New Delhi, India, and* [3]*Defence R&D Organization, Ministry of Defence, Government of India, Rajaji Marg, New Delhi, India*

(*Received date: 11 March 2010; In revised form date: 29 April 2010*)

Abstract

Mitochondrial DNA plays an important role in cellular sensitivity to cancer therapeutic agents. Hoechst 33342, a DNA minor groove binding ligand, has shown radiosensitizing effects in different cancer cell lines. In the present study, the possible binding of Hoechst 33342 with mitochondrial DNA, isolated from human cerebral glioma (BMG-1) cells, was investigated and consequences of this binding on excessive reactive oxygen species (ROS) generation in irradiated BMG-1 cells were studied. Alteration in the fluorescence spectroscopic characteristics of Hoechst 33342 suggested binding of Hoechst 33342 with isolated mitochondria and mitochondrial DNA. Persistent increase in level of ROS in the presence of Hoechst 33342 has been observed, which was further enhanced in irradiated cells. Investigations using inhibitors of ETC complex I suggested that mitochondrial bound Hoechst 33342 contributed to increased ROS, which was associated with alteration in ΔΨm and antioxidant machinery. These factors appeared to contribute in potentiating radiation-induced cell death in BMG-1 cells. The finding from these studies will be useful in designing better anti-cancer strategies.

Keywords: *Hoechst 33342, mtDNA, reactive oxygen species, radiosensitization*

Abbreviations: *mtDNA, Mitochondrial DNA; ROS, Reactive Oxygen Species; ΔΨm, Mitochondrial membrane potential; SOD, Superoxide oxide dismutase; FCCP, Carbonyl cyanide p-trifluoromethoxyphenylhydrazone; DPI, Diphenyleneiodonium chloride; DCFDA, 2',7' Dichlorofluorescein diacetate; DHE, Dihydroethidium; PI, Propidium iodide; JC-1, 5,5', 6,6'–tetrachloro-1,1', 3,3'-tetraethylbenzimidazolylcarbocyanine iodide; NAO, 10-N-nonyl acridine orange; ETC, Electron transport chain; NAC, N-acetyl cystein; HBSS, Hanks balanced salts solution*

Introduction

Hoechst 33342 is a bisbenzimidazole family molecule and binds with the AT rich region in DNA minor groove. This class of molecules have anti-cancer properties [1]. Most of the understanding of the observed cytotoxicity is centred around its inhibitory role on topoisomerases [1,2]. Several other cellular consequences like decrease in the formation of normal TATA box-binding protein/TATA box complexes [3], accumulation of endogenous E2F-1 (transcription factor) and a transient increase in the formation of high-molecular weight protein/E2F-1/DNA complexes in BC3H-1 myocytes and HL-60 cells are reported and linked with Hoechst 33342 induced apoptosis [4]. Hoechst 33342 also demonstrated radiosensitization of various human malignant cells [5]. However, the cellular radiation responses mediated by Hoechst 33342 in different cell systems were heterogeneous in nature.

Various studies have clearly demonstrated its high binding affinity with the AT rich minor groove region of DNA and the detailed nature of interaction of Hoechst mostly with nuclear DNA is available [6–8].

Correspondence: Rajeev Varshney, 339, DRDO Bhawan, Defence R&D Organization, Ministry of Defence, Government of India, Rajaji Marg, New Delhi 110 105, India. Tel: +91-11-23014873. Fax: +91-11-23014259. Email: rvarshney@rediffmail.com

ISSN 1071-5762 print/ISSN 1029-2470 online © 2010 Informa UK Ltd.
DOI: 10.3109/10715762.2010.492829

However, studies have not addressed at all its possible interaction with mitochondrial DNA, possessing many AT rich sites coding for various sub-units of redox carriers of electron transport of mitochondria, which are essential for its optimal function. Therefore, it is suggested that it may bind to AT rich sites in mitochondrial DNA and could alter events operating at the mitochondria level. It has been reported that mtDNA plays an important role in cellular sensitivity to cancer therapeutic agents [9]. This was also indicated from the recent reports on Hoechst 33342 induced apoptosis as a result of mitochondrial dysfunction [10]. Hoechst 33342 also inhibits fatty acid synthase (FAS) and its transcription, which is the sole enzyme responsible for *de novo* biosynthesis of fatty acids [11]. Therefore, it is hypothesized that alterations in transcription of sub-units essentially coded by mitochondrial DNA and inhibition of FAS would alter the membrane architecture which is essential for optimum functions of a redox carrier at inner mitochondrial membrane involved in electron transport. These alterations in membrane architecture would affect the reduction of oxygen through ETC, leading to more leakage of electrons, which may cause oxidative insult due to an increase in ROS resulting into mitochondrial dysfunction and cell death. Various anti-cancer agents like cisplatin and zidovudine are DNA interacting molecules and have been demonstrated to interact with mtDNA vis-a-vis increase in ROS-mediated mitochondrial dysfunction and increase in cytotoxicity [12]. Therefore, it is suggested that, in addition to inhibition of topoisomerase and accumulation of E2F-1 transcription factor, binding of Hoechst 33342 with mitochondrial DNA would also enhance the radiation-induced death of malignant cells through an increase in ROS mediated events and mitochondrial dysfunction.

The present study was carried out with malignantly transformed human glioma cells (BMG-1). Binding of Hoechst 33342 with mitochondrial DNA, isolated from human cerebral glioma (BMG-1) cells, was investigated using fluorescence spectroscopy and a consequence of this binding on excessive ROS generation in irradiated BMG-1 cells was studied. The results clearly indicated the enhanced radiation sensitivity of malignantly transformed glioma cells due to increase in ROS by Hoechst 33342. The finding from these studies will provide useful insight for understanding DNA minor groove binders mediated modification of radiation response and could aid in designing of more effective and better anti-cancer strategies.

Materials and methods

Cells

An established cell line human cerebral glioma (BMG-1) was used [13]. Cells were maintained as monolayer cultures at 37°C in a humidified CO_2 incubator (5% CO_2, 95% air) in 25 cm^2 tissue culture flasks. Cells were maintained in Dulbecco's Modified Eagles Medium (DMEM) supplemented with 5% foetal bovine serum (FBS), 10 mM HEPES and antibiotics (30 μg/ml penicillin G, 50 μg/ml streptomycin and 2 μg/ml nystatin). All treatments were carried out in exponentially growing cells. DMEM and FBS were purchased from Sigma Chemicals (Saint Louis, Missouri, USA).

Hoechst 33342 and γ-irradiation

Monolayer BMG-1 cells were grown for 24 h (exponential growth phase) before treatment in DMEM containing 5% foetal bovine serum. All treatments were carried out in Hank's balanced salt solution (HBSS) containing 5 mM glucose, which does not support growth. Hoechst 33342 was added to this liquid holding media (HBSS) 1 h before the irradiation and then replaced by growth media after radiation treatment. A ^{60}Co gamma radiation source (Co Teletherapy Model ELDORADO 78, AECL, Chalk River, Ontario, Canada) was used for irradiation at a dose rate 0.82–0.75 Gy/min. Cells were grown at 37°C following treatment and harvested at designated time intervals for measurement of various cellular response parameters.

Isolation of mitochondria from cells

The mitochondrial fraction was isolated by differential centrifugation using a mitochondria isolation kit (MITOISO2, Sigma-Aldrich, Saint Louis, Missouri, USA) according to the manufacturer's protocol. The mitochondrial purity and integrity was assessed by cytochrome c oxidase activity kit (CYTOCOX1, Sigma). Protein concentration of mitochondrial fraction was estimated using BCA protein assay kit (Pierce, Rockford, IL, USA). The mitochondrial fraction (60 μg) was incubated with Hoechst 33342 (5 μM) for 1 h in phosphate buffer saline (PBS) for binding studies using fluorescence spectroscopic measurements.

Purification of mitochondrial DNA from mitochondria

Approximately 2×10^8 cells were used to isolate the mitochondria according to the above procedure. Mitochondrial DNA (mtDNA) was extracted from the isolated mitochondria by a modified method of alkaline lysis procedure [14]. Briefly, isolated mitochondria were resuspended in freshly prepared 0.18 N NaOH containing 1% sodium dodecyl sulphate (SDS), vortexed and stored on ice for 5 min. An ice cold solution of potassium acetate (3 M potassium and 5 M acetate) was added, vortexed and stored on ice for an additional 5 min. The mixture was centrifuged at 12 000 g for 5 min at 4°C.

An equal volume of phenol-chloroform mixture was added in supernatant, mixed thoroughly by vortexing and then centrifuged at 12 000 g for 2 min at room temperature. The aqueous phase was transferred to a fresh tube and to this two volumes of ethanol were added, mixed by vortexing and kept at room temperature for 15 min. This mixture was centrifuged at 12 000 g for 5 min at room temperature, the resulting pellet of mtDNA washed with 1 ml of 70% ethanol and dried at room temperature. The mtDNA pellet was resuspended in an appropriate volume of 10 mM Tris-HCl buffer (pH 8.0), containing 1 mM EDTA and 20 μg/ml RNase. The purity of mtDNA was determined spectrophotometrically (Model Cary Bio 100, Varian, Mulgrave, VIC, Australia) by measuring the absorbance ratio at 260/280 nm. The value obtained was in the range 1.9–2.0 and binding characteristics of Hoechst 33342 (5 μM) with mtDNA (20 nM) were studied by fluorescence spectroscopy.

Fluorescence spectroscopic measurements

The fluorescence emission measurements were carried out using an integrated steady state fluorescence spectrofluorimeter (Model FS900) and fluorescence lifetime instrument (Model FL900CDT) from Edinburgh Analytical Instruments (Edinburgh, UK). The excitation source for spectral measurements was a xenon lamp. The samples were kept in 1 ml quartz cuvette and excited at 360 nm. The emission range was 375–600 nm. All other scanning parameters were optimized to obtain good spectra. The anisotropy measurements were performed using a pair of motorized Glan-Thompson prisms. The emission spectra in all four directions were recorded sequentially and used for calculation of anisotropy. The detailed procedures for these spectral measurements are adopted as mentioned in our earlier paper [15].

Flow cytometric measurement of ROS

Intracellular ROS generation was measured by flow cytometry using DCFH-DA (Sigma) according to the procedure described earlier [16]. Briefly, following treatment at specific time points, cells were washed with PBS and incubated with DCFH-DA (10 μg/ml) at 37°C for 30 min in the dark. Cells were then washed, scraped gently and resuspended in PBS and kept on ice for an immediate detection by flow cytometry (FACS-Calibur, Becton Dickinson, San Jose, CA, USA) using the argon laser (488 nm) for excitation. Green fluorescence due to intracellularly trapped DCF was collected on the FL1 channel on log scale. Data was acquired and analysed using the CELL Quest programme (Becton Dickinson). The cells were also stained separately with dihydroethidium (10 μM), a superoxide specific dye in HBSS [16,17]. The dihydroethidium oxidized to ethidium upon reaction with superoxide and emits red fluorescence emission at 590 nm on binding with DNA, which is collected on FL2 channel on log scale.

Macrocolony assay

Cells (150–600, depending upon the treatment) were plated in 60 mm Petri dishes in triplicate at a uniform density. After 24 h of plating cells were treated with Hoechst 33342 for 1 h followed by irradiation by ^{60}Co gamma radiation and then incubated at 37°C in a 5% CO_2 humidified atmosphere for 8–10 days to allow colony formation. Colonies were fixed with methanol and stained with 1% crystal violet. Colonies containing more than 50 cells were counted; plating efficiency (PE) and surviving fraction (SF) was calculated as:

$$PE = [\text{No. of colonies/No. of cells plated}] \times 100,$$
$$SF = PEt/PEc$$

where PEt is plating efficiency after treatment and PEc is plating efficiency of control.

Cell proliferation and cell cycle analysis

Exponentially growing BMG-1 cells were seeded at 1×10^5 cells/Petri dish of 35 mm diameter for growth kinetics studies. Immediately after irradiation (5 Gy) in the presence and absence of Hoechst 33342 (5 μM), cells were harvested at every 24 h upto 72 h by trypsinization and counted using a haemocytometer. For determining the proliferation (N_t/N_0), where N_0 is the total number of cells at the time of treatment and N_t is the total number of cells at time t. Progression of cells through different phases of cell cycle was also measured flow cytometricaly along with growth kinetics. Both floating and attached cells were counted and fixed in 80% chilled ethanol for cell cycle analysis. Cellular DNA content was measured in ethanol fixed cells using the intercalating DNA fluorochrome, propidium iodide (PI) as described earlier [18]. The cells ($0.5–1 \times 10^6$) were washed with PBS after removing ethanol and treated with RNase A (200 μg/ml) for 30 min at 37°C. Subsequently cells were stained with PI (25 μg/ml) for 15 min at room temperature. Measurement were made with an argon laser-based flowcytometer (FACS-Calibur, Becton Dickinson) using the argon laser (488 nm) for excitation. Distribution of cells in different phases of cell cycle was calculated from the frequency distribution of DNA content by using the Mod fit Programme (Variety Software, CA).

Micronuclei analysis

Air-dried slides of acetic acid/methanol fixed cells were stained with a DNA specific dye, diamidino-2-phenylindole dihydrochloride, DAPI (10 μg/ml) in

citric acid (0.1 M), disodium phosphate (0.5 M) and buffer containing 0.5% Tween-20 for 30 min in the dark. Approximately 1×10^3 cells were analysed from duplicate slides. Data were analysed by obtaining integrated values of micronuclei frequency and normalizing the values with respect to cell numbers. Frequency of the cells with micronuclei, called the M Fraction (MF) was calculated as:

$$\text{MF } (\%) = Nm/Nt \times 100,$$

where Nm = number of cells with micronuclei and Nt = total number of cells analysed.

Annexin V binding

Apoptotic cells were detected by the labelling of externalized phosphotidylserine using annexin V-FITC in unfixed cells [19]. Following treatment cells were harvested and aliquots of 1×10^5 cells resuspended in 100 µl binding buffer (10 mM HEPES/NaOH, pH 7.4, 10 mM NaCl, 2.5 mM $CaCl_2$) and 5 µl annexinV-FITC and 10 µl PI (50 µg/ml) were added. After 15 min of incubation at room temperature 400 µl of binding buffer were added to each sample and analysed by flow cytometry. The percentage of annexin V-positive and negative cells were estimated by applying appropriate gates and using the regional statistics analysis facility provided in the CELL Quest programme (Becton Dickinson).

Mitochondrial membrane potential estimation by flow cytometry and confocal microscopy

Mitochondrial membrane potential was studied using the potentiometric dye rhodamine123 and 5,5',6,6'-tetrachloro-1,1', 3,3'-tetraethylbenzimidazolylcarbocyanine iodide (JC-1) [20]. At indicated time points treated cells were incubated with 5 µM rhodamine 123 (Sigma). After incubation for 30 min at 37°C in the dark, cells were washed with ice-cold PBS, scraped and transferred immediately in a flow tube kept at ice temperature until measurement. Cells were also treated with FCCP (50 µM) for 2 h prior to rhodamine staining and considered as a positive control. Rhodamine123 was excited at 488 nm and emits green fluorescence at 534 nm measured by flow cytometry.

Further $\Delta\psi$m was studied using JC-1 dye by a confocal microscope (Model LSM 510, CARL ZEISS, Jena, Germany). JC-1 is a membrane potential sensitive dye, considered as a reliable and sensitive fluorescent probe for detecting differences in $\Delta\psi$m due to its dual emission characteristics. Briefly, cells were grown on cover slip at a density of 1×10^5 cells. At 72 h after irradiation cells were stained with JC-1 (2 µM) in DMEM containing 5% foetal bovine serum at 37°C for 25 min. Following staining, coverslips were washed with cold PBS and placed on glass microscope slides and examined immediately. At low concentrations JC-1 exists mainly in a monomeric form, emitting green fluorescence (emission maximum at ~ 530 nm). At high concentrations this molecule forms aggregates, known as J-aggregates and emits orange–red fluorescence (emission maximum at ~ 590 nm). JC-1 was excited at 488 nm from a low power argon laser in a confocal microscope. JC-1 green fluorescence was visualized with a long-pass filter (LP505) and red fluorescence from JC-1 aggregates was detected using a long-pass filter (LP560). Necessary care was taken to block the red spectral region from the long-pass filters (LP505) by using the NFT filters in the beam path. The images were recorded with a 40× oil immersion objective. Since the amount of cationic dye taken up by the mitochondrion depends on its trans-membrane potential, at low $\Delta\psi$m the fluorescence emission will be mostly green, whereas at high $\Delta\psi$m it will shift to orange–red due to more uptakes within mitochondria. $\Delta\psi$m was also measured flow cytometrically by using JC-1 fluorescence dye.

Mitochondrial mass

Mitochondrial mass was assessed using the fluorescent dye 10-N-nonyl acridine orange (NAO) and binds specifically with unoxidized cardiolipin [21]. Cells were washed twice with PBS and incubated with 2 µM NAO for 20 min at 37°C in the dark. Cells were then washed, resuspended in PBS and transferred immediately to flow tubes kept on ice for immediate flow cytometry measurements. Fluorescence was collected on the FL1 channel on a log scale. A minimum of 1×10^4 cells per sample was analysed. Data was acquired and analysed using the CELL Quest programme (Becton Dickinson).

Mn-SOD activity determination

Mn-SOD activity was determined by a spectrophotometric method using the SOD assay kit (Cayman Chemicals, Ann Arbor, MI, USA) according to the manufacturer's protocol. This kit utilizes a tetrazolium salt for detection of superoxide radicals generated by xanthine oxidase and hypoxanthine. One unit of SOD is defined as the amount of enzyme needed to exhibit 50% dismutation of the superoxide radicals. Potassium cyanide (3 mM) was added to the assay which inhibits Cu/Zn SOD, resulting in the detection of only Mn-SOD activity. Cellular protein was measured using the BCA protein assay kit (Pierce, Rockford, IL, USA) according to the manufacturer's protocol and enzyme activity was normalized to cellular protein.

Catalase activity determination

Catalase activity was determined by a spectrophotometric method using the catalase assay kit (Cayman

Chemicals) according to the manufacturer's protocol. In brief, this kit utilizes the peroxidatic function of catalase for determination of enzyme activity. The method is based on the reaction of the enzyme with methanol in the presence of optimal concentration of H_2O_2. The formaldehyde produced is measured spectrophotometrically with 4-amino-3-hydrazino-5-mercapto-1,2,4-triazole (Purpald) as chromogen. Purpald specifically forms a bicyclic heterocycle with aldehyde, which upon oxidation changes from colourless to a purple colour. Cellular protein was measured using the BCA protein assay kit (Pierce) and enzyme activity was normalized to cellular proteins.

Western blot analysis of Mn-SOD and catalase

Treated cells were washed with PBS, scraped, centrifuged at 600 g for 5 min and cell pellets were subsequently lysed by adding lysis buffer (50 mM HEPES, 55 mM KCl, 1% Triton X, 1 mM Na_3VO_4, 50 mM NaF, 1 mM PMSF, 1 mM Benzamidine) and protease inhibitor cocktail and kept on ice for 20–30 min. Lysed cellular extract was centrifuged at 15 000 g for 20 min at 4°C. Protein concentration was estimated using BCA estimation kit (Pierce). Equal amounts (40 μg) of total protein were analysed by electrophoresis in a 12% SDS-polyacrylamide running gel and a 5% stacking gel. The proteins were then electrotransferred onto PVDF membrane. After blocking in 5% skimmed milk for 1 h, membranes were washed with Tris-buffer saline (TBS) containing 0.1% Tween and then treated with specific antibodies of Mn-SOD and Catalase (1:200 to 1:2000 dilution) for 1 h. These antibodies were obtained from Santa Cruz Biotechnology (Santa Cruz, CA). The blots were incubated with horseradish peroxidase-conjugated bovine anti-goat IgG (1:2000) for 1 h at room temperature. Washed blots were then treated with an enhanced chemiluminescence western blot detection solution (Amersham Life Science, Buckinghamshire, UK) and exposed to X-ray film. The quantitative analysis of Mn-SOD and catalase level in each sample was carried out using Image Quant analysis software tool (Molecular Dynamics, Inc., Sunnyvale, CA, USA).

Statistical analysis

Data were presented as means ± SD. Differences between multiple groups were examined by using ANOVA followed by *post-hoc* test (SPSS package). A value of $p < 0.05$ was considered significant.

Results

Possible binding sites of Hoechst 33342 in mtDNA

DNA footprinting and biophysical studies have shown strong binding preference of Hoechst for AT sequences with a binding site size of 4–5 bases [6,8,22]. Mitochondrial DNA possesses many AT rich sites in different genes coding for sub-units of redox carriers of electron transport. Number of AT rich region up to four base pair (ATAT) in various genes was calculated manually from the double strand sequence of mtDNA available in the revised Cambridge research sequence [23]. The total number of ATAT rich regions present in the different genes was calculated and represented in parentheses (Figure 1A). Hoechst 33342 can bind with these AT sites in mitochondrial DNA.

Binding of Hoechst 33342 with isolated mitochondria and mtDNA

Steady state fluorescence and excited state fluorescence life time measurements were carried to assess the binding of Hoechst 33342 with mtDNA in the following different experimental conditions; (i) Mitochondria isolated from BMG-1 cells pre-treated with 5 μM Hoechst 33342 and (ii) in isolated mitochondria treated with Hoechst 33342 (Figure 1B). Finally, spectral measurements of Hoechst 33342 were carried out with isolated mtDNA. Similar measurements were also carried out with Hoechst 33342 in phosphate buffer alone (without DNA). Spectral data (emission maximum, anisotropy and fluorescence lifetimes) obtained are in concurrence with our earlier data of Hoechst 33342-calfthymus DNA in phosphate buffer solutions (Table I).

The emission maximum at 503 nm in phosphate buffer shifted to 470 nm in isolated mitochondria from cells pre-treated with Hoechst 33342 (Figure 1B). A similar spectral shift was observed in isolated mitochondria treated with Hoechst 33342. The intensity of emission at 470 nm was also increased as compared to Hoechst 33342 alone in PBS (Figure 1B). Further, an increase in emission anisotropy of 0.3 was observed in the experimental conditions mentioned above as compared to 0.14 in PBS (Table I). Fluorescence lifetime measurements provide direct evidence of bound state of a fluorescent molecule with macromolecule. Fluorescence lifetimes of Hoechst is double exponential in nature with short (τ_1) and long (τ_2) decay components and their numerical values are 0.2 ns and 4.1 ns, respectively (Table I). The short component (τ_1) increases upon binding with DNA from 0.2 ns to 2.1 ns. Thus, in mitochondria the observed decay components of excited state lifetimes of 2.1 ns (τ_1) and 3.8 ns (τ_2) indicate bound state. Their relative contributions also systematically altered in the fluorescence decay profiles. Hoechst 33342-mtDNA showed an emission maximum at 460 nm, anisotropy at 0.28 and short and long decay components at 1.31 ns and 3.6 ns. These measured values are similar to Hoechst 33342-calfthymus DNA in phosphate buffer (Table I). The detailed comparison of measured fluorescence spectral parameters clearly indicated

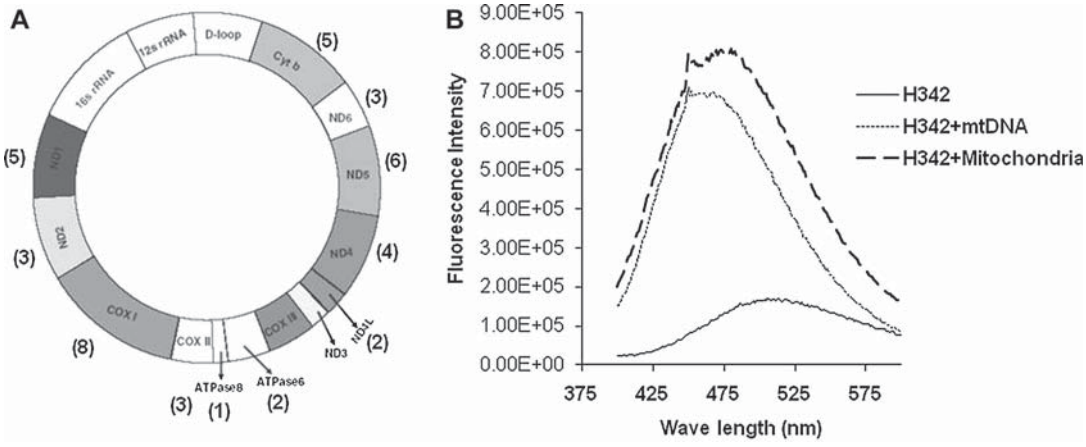

Figure 1. Number of binding sites of Hoechst 33342 (H342) in mitochondrial genome and fluorescence spectroscopic measurements of Hoechst 33342 with mitochondria and mtDNA. (A) Mitochondrial genome showing number of AT rich region up to four base pair (ATAT) in various mitochondrial genes (number indicated in parenthesis). (B) Fluorescence emission spectra of Hoechst 33342 (5 μM) with isolated mitochondria (long thick dashed line), with mtDNA (thin dotted line) and Hoechst 33342 alone in phosphate buffer saline (thin continuous line). In order to compare the spectral changes under different measuring conditions, the intensity scale for thin dotted line and thin continuous line was multiplied by 10. The emission maximum of Hoechst 33342 with mitochondria and mtDNA are observed at 470 nm and 460 nm, respectively. The corresponding emission maximum of Hoechst 33342 in phosphate buffer saline was at 503 nm.

binding of Hoechst with mtDNA in mitochondria of BMG-1 cells (Table I). This binding may impair the functions of the electron carriers for reduction of oxygen through ETC. Therefore, further studies have been designed to investigate the consequence of this binding in BMG-1 cells.

ROS generation

Intracellular ROS generation was assessed by flow cytometry using ROS marker DCFH-DA. A time-dependent accumulation in ROS was observed up to 72 h when cells were irradiated (5 Gy) in the presence of Hoechst 33342 (5 μM). An increase (2–3-fold) in ROS production was observed with irradiation (5 Gy) and an almost similar increase was observed with Hoechst 33342 (5 μM). However, the presence of Hoechst 33342 enhanced the ROS production further, up to 4–5-fold at 72 h in irradiated cells (Figure 2A). The histogram showing the effect of this treatment at 72 h on ROS production is shown in Figure 2B. The level of ROS generation was further probed by using superoxide specific probe, dihydroethidium. A similar increasing trend in superoxide radical has been observed in treated cells (Figure 2C). An increase in production of superoxide radicals induced by Hoechst 33342 in irradiated cells has been observed. Further, these measurements clearly demonstrated that Hoechst 33342-induced ROS generation persists for a longer duration both in the presence of Hoechst 33342 alone and with radiation in BMG-1 cells.

Effects of ETC complex I inhibitors on Hoechst 33342-induced ROS generation

In the earlier section, we have shown the Hoechst 33342 is able to bind with mtDNA. Therefore, to examine the influence of Hoechst 33342 on ROS production through mitochondrial electron transport chain redox carrier, the effects of rotenone and diphenyleneiodonium chloride (inhibitors of complex I) on ROS generation were studied. The extent of ROS generation at 24 h

Table I. Emission maximum, anisotropy and fluorescence life times of Hoechst 33342 with isolated mitochondria and mtDNA showing binding of Hoechst 33342 (H342) with mitochondrial DNA.

Treatment	Emission max. (nm)	Anisotropy at 500 nm	Fluorescence life times (τ) of H342 with isolated mitochondria, mtDNA and calf thymus DNA				
			τ_1 (ns)	A1 (%)	τ_2 (ns)	A2 (%)	χ^2
H342 in PBS	503	0.14	0.2	54	4.1	46	0.92
Mitochondria of H342 treated cells	470	0.3	2.1	62	3.8	38	0.7
Mitochondria treated with H342	468	0.26	2.2	73	4.4	27	0.87
H342+mtDNA	460	0.28	1.31	37	3.6	63	0.79
H342+Calf thymus DNA	473	0.29	2.4	52	4.4	48	0.98

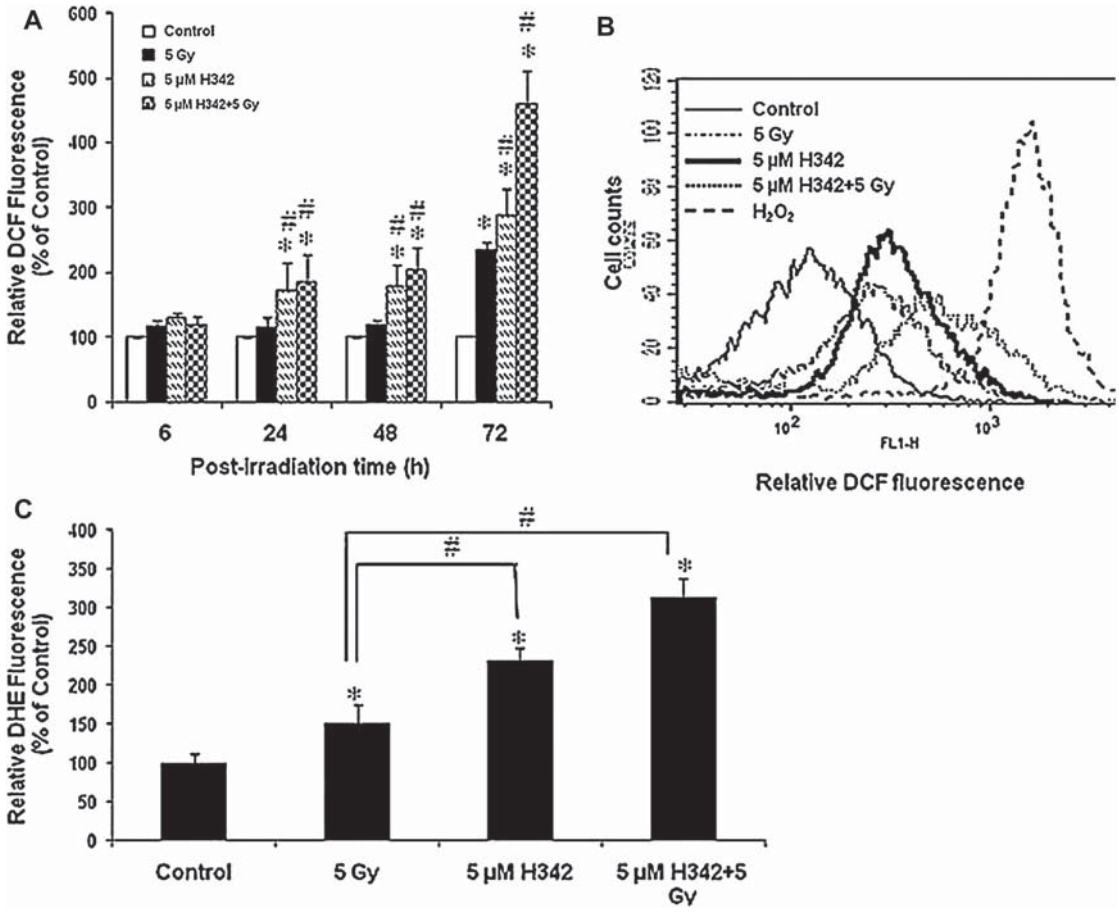

Figure 2. Effects of Hoechst 33342 (H342) on ROS levels in gamma irradiated BMG-1 cells. (A) Time-dependent increase in intracellular ROS level measured by DCF fluorescence. Values represent the means ± SD of three independent experiments. $^{*}p < 0.05$ vs control. $^{\#}p < 0.05$ vs 5 Gy. (B) Representative histogram showing ROS levels in the presence and/or absence of Hoechst 33342 in irradiated BMG-1 cells at 72 h, H_2O_2 (0.5 M) added 10 min before DCF measurement used as a positive control. (C) A similar increasing trend in superoxide radical followed in treated cells measured at 48 h using superoxide specific dye dihydroethidium (DHE).Values represent the means ± SD of three independent experiments. $^{*}p < 0.05$ vs control. $^{\#}p < 0.05$ (5 Gy vs 5 μM H342 and 5 μM H342+5 Gy).

after co-treatment of rotenone (0.2 μM) and diphenyleneiodonium chloride (1 μM) with Hoechst 33342 was assessed by the flow cytometer. Figure 3 shows that the co-treatment with these inhibitors of complex I inhibited the Hoechst-induced ROS generation by ~75%. Hoechst 33342-treated irradiated cells also showed similar extent of inhibition. The treatment with these inhibitors alone decreased the endogenous level of ROS by 20–45%. The result indicated the contribution of Hoechst in the induction of ROS production through ETC. The results were further substantiated by using mitochondrial ROS specific probe dihydrorhodamine (2 μM). Hoechst 33342 (5 μM) increased fluorescence of dihydrorhodamine by ~ 40% at 24 h after treatment indicated enhanced generation of ROS through mitochondrial ETC (data not shown).

Cell survival

Dose–response of gamma-ray-irradiated exponentially growing BMG-1 cells was earlier observed in our lab [24]. Loss of clonogenicity as a function of radiation dose (2 and 5 Gy) and Hoechst concentration (0.1–10 μM) has been observed (Figure 4A). Hoechst 33342 (5 μM, IC_{50}) significantly lowered the survival of gamma ray irradiated (5 Gy) BMG-1 cells additionally by 30–40% (Figure 4A). These observations are similar to earlier studies from our laboratory [5]. Treatment of cells with Hoechst 33342 (5 μM) decreased survival by 50%, which was restored up to 80% when cells were incubated with N-acetyl cysteine (NAC, 10 mM) for 3 h (Figure 4B). Irradiation of Hoechst 33342-treated cells in the presence of NAC similarly enhanced the compromised survival, suggesting the contribution of ROS in Hoechst 33342-induced cell death.

Growth delay and cell cycle perturbations

To investigate the nature of perturbations in cell cycle progression induced by Hoechst 33342 in combination with radiation, growth kinetics and cell cycle analysis were studied. Both irradiation (5 Gy) and Hoechst 33342 (5 μM) inhibited growth of BMG-1

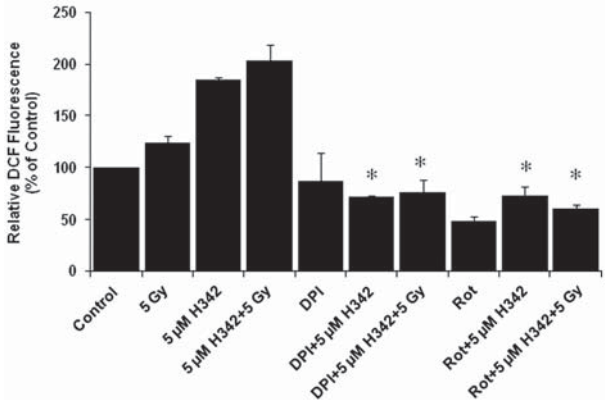

Figure 3. Effects of mitochondrial ETC complex I inhibitors on the Hoechst 33342 (H342)-induced ROS production. Rotenone (Rot), 0.2 μM and diphenyleneiodonium chloride (DPI), 1 μM were co-incubated with Hoechst 33342 for 1 h following irradiation and ROS measured at 24 h after irradiation in cells. These inhibitors inhibited the Hoechst 33342-induced ROS production in irradiated and un-irradiated cells. Values represent the means ± SD of three independent experiments. $^{*}p < 0.05$ vs respective treatment without ETC inhibitors.

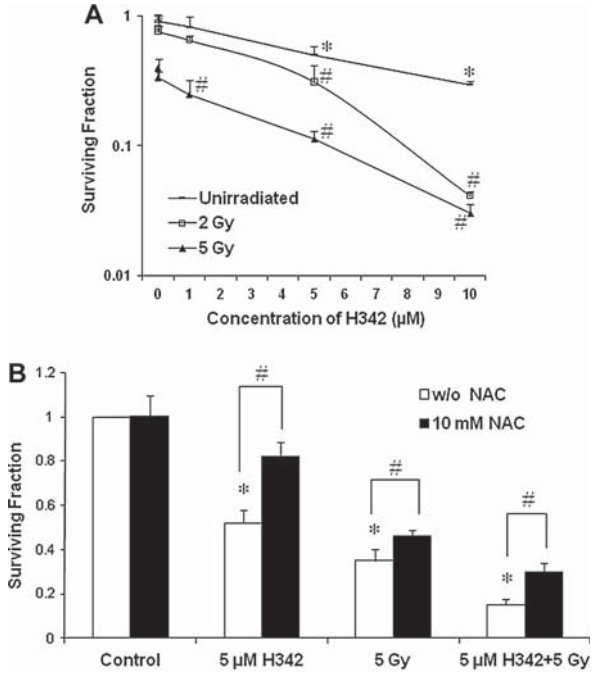

Figure 4. Hoechst 33342 (H342)-induced ROS mediated cell death measured by clonogenic assay. (A) Effects of concentration of Hoechst 33342 (0.1–10 μM) on the survival of irradiated (2 and 5 Gy) BMG-1 cells. Values represent the means ± SD of three independent experiments. $^{*}p < 0.05$ vs control; $^{\#}p < 0.05$ vs respective radiation dose without Hoechst 33342. (B) Increase in cell survival was observed in the presence of N-acetyl cysteine (NAC, 10 mM) following treatment. Cells were incubated for 7–8 days for colonies formation and stained with 1% crystal violet. Colonies containing more than 50 cells were counted. Values represent the means ± SD of three independent experiments $^{*}p < 0.05$ vs control; $^{\#}p < 0.05$ (treatment without NAC vs respective treatment with NAC).

cells to a similar extent with time (50–70%). Irradiation in the presence of Hoechst 33342 (5 μM) showed a sub-additive effect on the growth inhibition (70–90%) (Figure 5A). Radiation (5 Gy) and Hoechst 33342 (5 μM) delayed the progression of cells through different phases of cell cycle which resulted in growth inhibition. DNA flow cytometric measurements further elucidated the nature of cell cycle perturbations. Hoechst 33342 (5 μM) and irradiation (5 Gy) independently caused G_2/M block and this effect was further enhanced when cells were irradiated in the presence of Hoechst 33342. A 2.3-fold increase in G_2/M phase cells was observed following irradiation (5 Gy) and/or with Hoechst 33342 after 48 h post-treatment. However, a more than 4-fold increase was observed in G_2/M phase when cells were irradiated in the presence of Hoechst 33342 at this time point. This trend was observed even up to 72 h (Figure 5B).

Cytogenetic death

Radiation causes both mitotic death (cytogenetic damage) as well as inter-phase death (mainly in the form of apoptosis). Therefore, an attempt was made to investigate the contribution of both mitotic death and apoptosis in the observed radiosensitization in BMG-1 by analysing the micronuclei induction. The percentage of cells with micronuclei (M-fraction), when the cells have completed one post irradiation doubling (between 24–36 h post-irradiation) as well as over all induction until 72 h were analysed. The frequency of micronuclei (M-fraction) in un-irradiated cells was in the range of 1–4%. The kinetics of micronuclei induction following an absorbed dose of 5 Gy showed a maximum frequency in the range of 22–28% between 24–48 h post-irradiation (Figure 6A). This was followed by a decline in the MF values due to the well-known dilution effects. Hoechst 33342 (5 μM) alone induced micronuclei frequency up to 4% (Figure 6A). Radiation in the presence of Hoechst 33342 further increased micronuclei formation (28–35%). These findings suggest that cytogenetic death has a significant contribution in radiation-induced cell death by Hoechst 33342.

Apoptosis

Externalization of phosphatidylserine on account of membrane asymmetry changes during apoptosis was probed using FITC-labelled annexin V [19]. Since Hoechst 33342 showed a significant increase in ROS after 24 h of treatment, annexin V positive cells were measured at a later time interval at 48 h. A significantly enhanced level of apoptotic cell death was observed with Hoechst 33342 alone and its combination with radiation. A significant increase in annexin V and PI positive cells was observed with 5 μM Hoechst 33342 (12%). Further increase up to 20% was observed in cells irradiated in the presence of Hoechst 33342 (Figure 6B). This was correlated with increased granularity of ~40%, higher side scatter

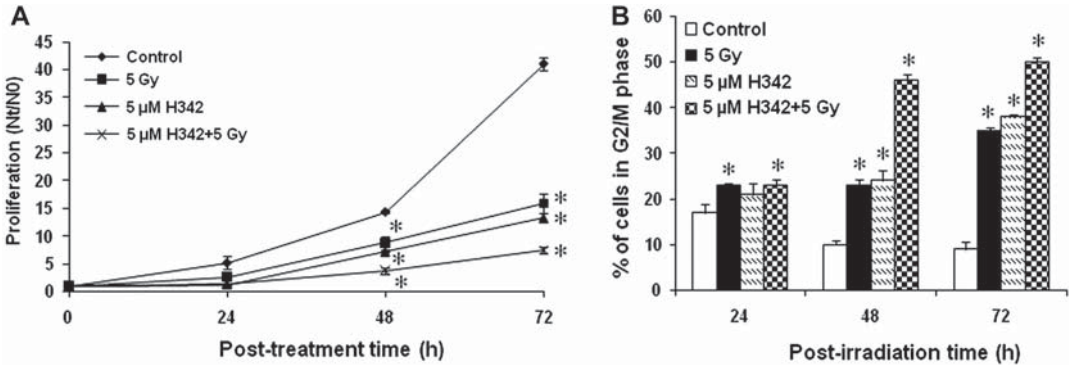

Figure 5. Effects of Hoechst 33342 (H342) on proliferation and cell cycle distribution of exponentially growing cells. (A) Time dependent (0–72 h) growth inhibition of un-irradiated and irradiated cells by Hoechst 33342. Value represent the means ± SD of three independent experiments. $^{*}p < 0.05$ vs control. (B) Bar diagram showing percentage of cells present in G_2 phase of cell cycle. Value represent the means ± SD of three independent experiments. $^{*}p < 0.05$ vs control.

(data not shown). The data then indicated the possible role of Hoechst 33342 in inducing the apoptotic death in irradiated cells as well.

Flow cytometric and confocal laser microscopic observations of mitochondrial membrane potential (Δψm)

The enhanced level of ROS is expected to alter the mitochondrial membrane potential (Δψm). Δψm was measured with the help of potentiometric dyes rhodamine-123 and JC-1 by flow cytometry and confocal laser microscopy. Mitochondrial membrane potential was measured at initial time points (2 and 4 h) and also at later time points (24, 48 and 72 h) to investigate the effects of Hoechst 33342-induced ROS on mitochondrial membrane potential of irradiated cells. A flow cytometric measurement of rhodamine 123 fluorescence is shown in Figure 7A. Treatment of cells with FCCP (50 μM), uncoupler showed a decrease in rhodamine fluorescence and were used as a positive control. There was no significant change observed at initial 2 h after treatment either with Hoechst 33342 (5 μM) or irradiation (5 Gy), while their combination marginally decreased the rhodamine fluorescence. However, at 4 h after treatment rhodamine fluorescence decreased by 25% and 45% following treatment of cells with irradiation (5 Gy) and Hoechst (5 μM), respectively, and their combination decreased fluorescence further by 60%. Interestingly, at later time points Hoechst 33342 increased the rhodamine fluorescence ~2–4-fold with time until 72 h, which is further enhanced when cells

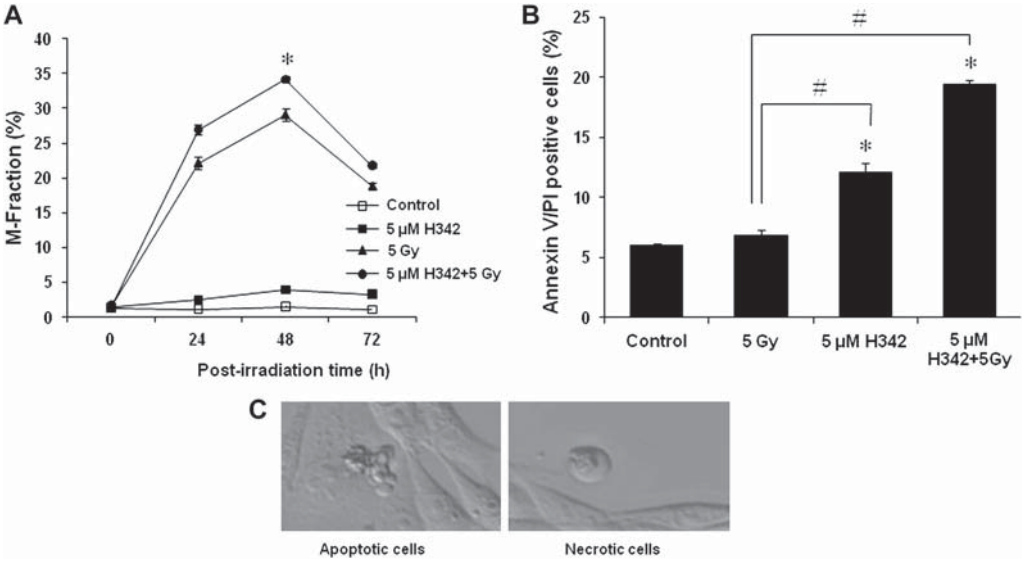

Figure 6. Hoechst 33342 (H342) enhanced both cytogenetic and apoptotic radiation-induced cell death. (A) Hoechst 33342 increased radiation induced micronuclei formation at 48 h. Values represent the means ± SD of two independent experiments. $^{*}p < 0.05$ vs radiation in absence of Hoechst 33342. (B) Hoechst 33342 enhanced cell death measured by annexin V and PI staining after 48 h of irradiation. Values represent the means ± SD of two independent experiments. $^{*}p < 0.05$ vs control. $^{\#}p < 0.05$ (5 Gy vs 5 μM H342 and 5 μM H342+5 Gy). (C) Morphological representation of cell death induced by Hoechst 33342.

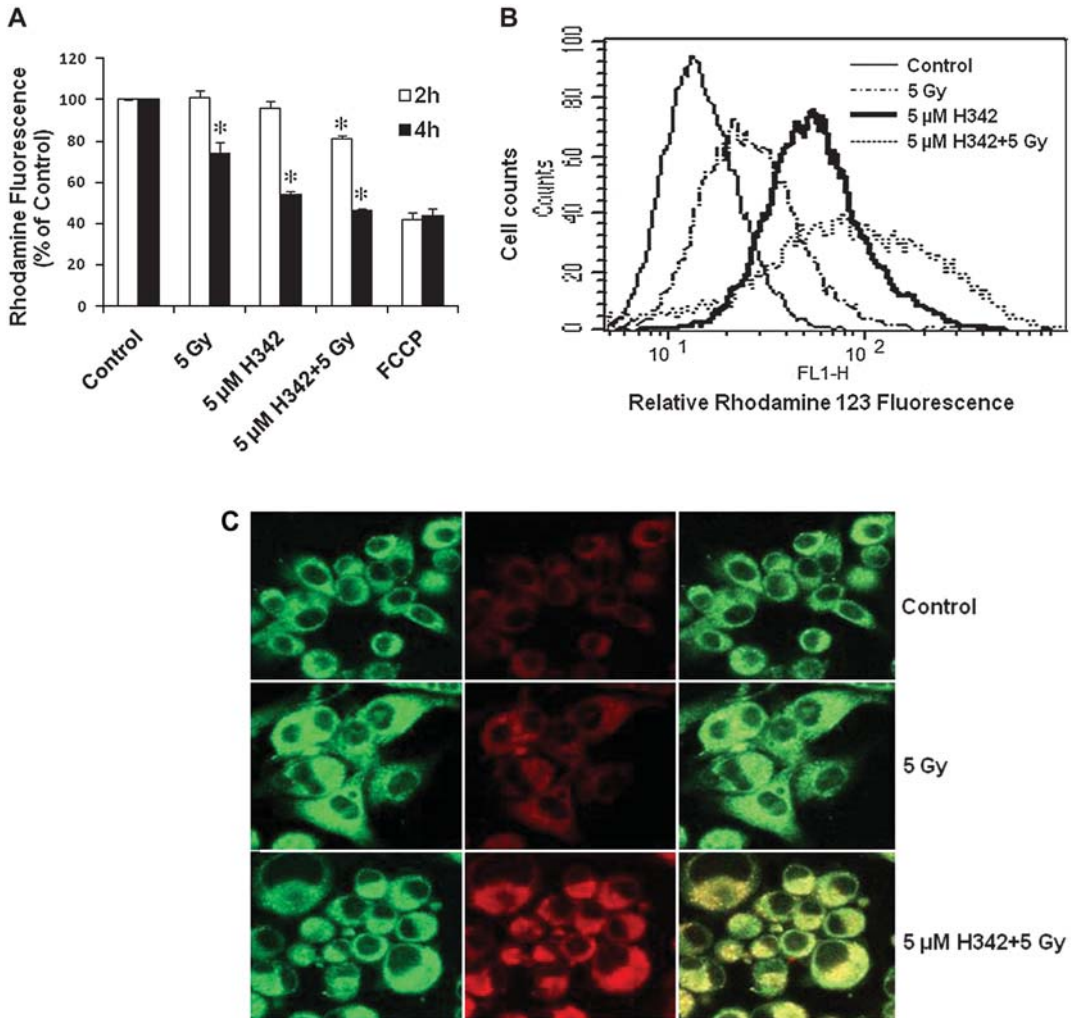

Figure 7. Mitochondrial membrane potential of gamma irradiated (5 Gy) BMG-1 cells in the presence and/or absence of Hoechst 33342. (A) Bar diagram showing the decreased membrane potential at early time points (2 and 4 h) by Hoechst 33342 and irradiation which is further decreased by their combination. FCCP (50 µM) used for collapse of membrane potential and considered as positive control. Value represents the means ± SD of three independent experiments. $^{*}p < 0.05$ vs respective controls. (B) Histogram showing increased membrane potential at 72 h by Hoechst 33342 and irradiation, which is further enhanced by their combination. Histogram is the best representative of three independent experiments. (C) Representative images of mitochondrial membrane potential using JC-1 dye observed under a confocal microscope at 72 h. Hoechst 33342 increased radiation-induced red fluorescence of JC-1 in mitochondria, showing hyperpolarization of mitochondria. Measuring conditions are described in Materials and methods.

were irradiated (5 Gy) in the presence of Hoechst 33342 (5 µM, data not shown). A typical histogram showing an increase in mitochondrial membrane potential (increased rhodamine fluorescence) at 72 h is depicted in Figure 7B. A similar increase in red fluorescence of JC-1 was observed in confocal microscope images due to an increase in mitochondrial membrane potential at 72 h (Figure 7C).

Hoechst 33342-induced activity and levels of Mn-SOD and catalase

An increase in ROS through alteration in activity of a redox carrier is expected to create oxidative stress in the vicinity of mitochondria and might alter the response of endogenous antioxidant enzymes. Intracellular antioxidant enzymes play an important role in the maintenance of redox homeostasis. The result showed that after 24 h post-treatment, Hoechst 33342 increases (1.5-fold) activity as well as level of Mn-SOD which act as a first line of defense against oxidative insult in mitochondria which was enhanced to 2-fold when the cells were irradiated in the presence of Hoechst 33342 (Figure 8A). On the other hand, the catalase activity and the protein level were marginally increased under similar experimental conditions (Figure 8B).

Discussion

Binding characteristics of Hoechst 33258 and its synthetic analogues with calfthymus DNA and oligonucleotides are well established through a variety of biophysical and computational tools [25–29].

Fluorescence spectroscopic characteristics like: (i) strong emission intensity enhancement, (ii) spectral shift of emission maximum to blue–green region, (iii) increase in anisotropy and (iv) altered fluorescence lifetimes, serve as spectroscopic markers and are routinely considered in binding studies [6,15,25–29]. The observed emission spectral position ca. 470–460 nm, increased value of emission anisotropy 0.3 and increased fluorescence lifetimes of short decay component at 2.1 ns of Hoechst 33342 with mitochondria and mtDNA compared to free Hoechst 33342 in buffer are clear evidence of bound Hoechst 33342 (Table I). Possible binding sites of Hoechst 33342 in the circular mtDNA suggest its implication in the alteration in transcription of various sub-units coded by mtDNA (Figure 1B). The persistent increase and accumulation of ROS at 72 h indicates the influence of binding of the Hoechst 33342 with the mtDNA (Figure 2). ROS is generated during the four-electron reduction of molecular oxygen to water for energy production. The partial reduction of molecular oxygen results in the production of superoxide and hydrogen peroxide [30]. Accumulation of ROS generated from the primary ionization events (5 Gy in Figure 2) was significantly low as compared to Hoechst 33342 treated cells, possibly due to its interference during subsequent cell divisions by affecting the transcription of various sub-units of redox electron carriers located in the inner mitochondrial membrane through mitochondrial transcription machinery. Hoechst is also known to inhibit fatty acid synthase and its transcription, the sole enzyme responsible for *de novo* biosynthesis of fatty acids in maintaining membrane architecture [11]. Inhibition of transcription of both, i.e. sub-units coded by mtDNA and FAS, contribute towards accumulation of delayed ROS through inefficient electron transfer at complex I. Inhibition of Hoechst 33342-induced ROS generation by ETC complex I inhibitors rotenone and DPI clearly indicates towards the generation of ROS through electron transport chain (Figure 3). This observation is similar to studies on the mechanisms of sulforaphane (an anticancer drug) induced mitochondrial ROS generation [31]. Therefore, the initial production of ROS might

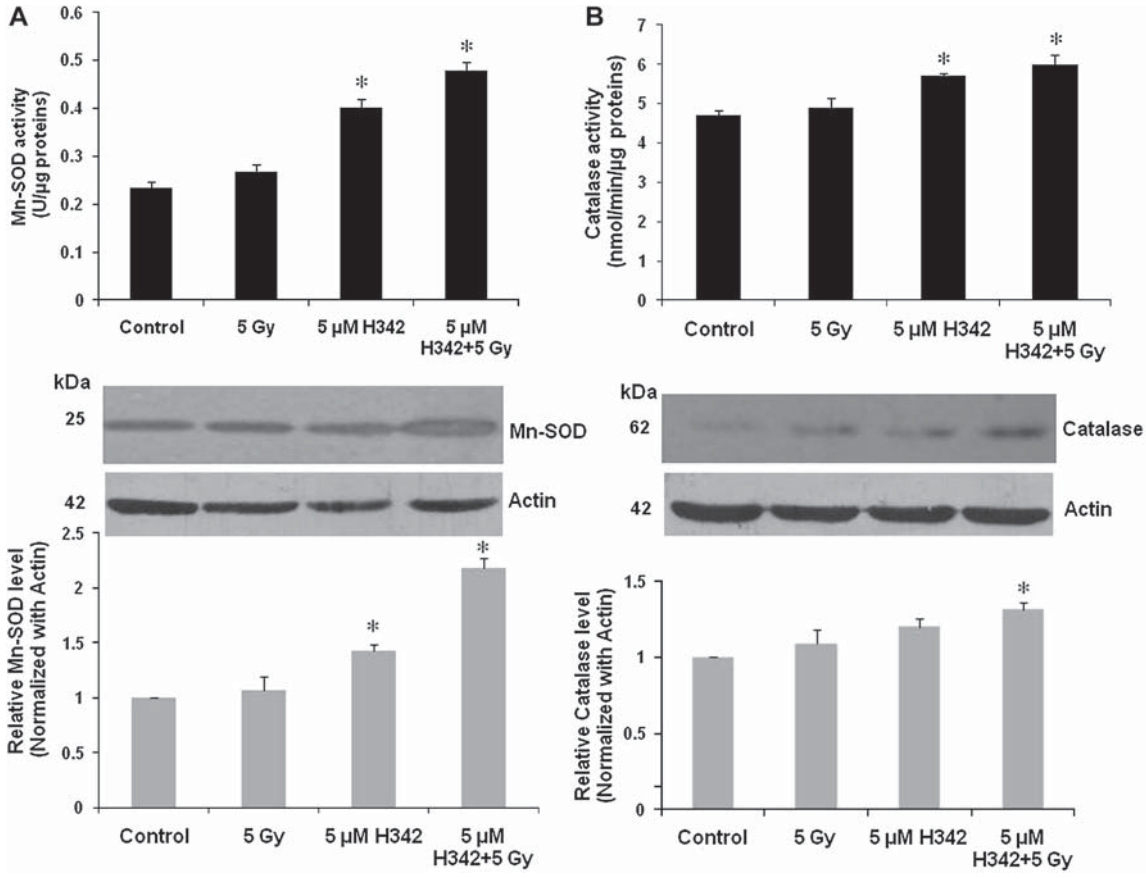

Figure 8. Antioxidant enzymes activity and protein levels in the presence and absence of Hoechst 33342 (H342) and irradiation (5 Gy). (A) Mn-SOD activity and protein level were increased at 24 h after Hoechst 33342 treatment and further enhanced in irradiated cells. Each bar represents the means ± SD of two independent experiments. $^{*}p < 0.05$ vs control. (B) Catalase activity and protein level were marginally increased at 24 h when cells were irradiated in the presence of Hoechst 33342. In the middle panel of (A) and (B), representative results of two independent experiments are shown. Data in the bottom panel of (A) and (B) represents the quantitative analysis of Mn-SOD and Catalase level, respectively, by densitometry. Each bar represents the means ± SD of two independent experiments. $^{*}p < 0.05$ vs control.

not entirely be responsible for the overall cellular effects of radiation, rather large ROS accumulation at later time due to the presence of Hoechst 33342 could be responsible for the fate of the irradiated cell population.

ROS initiates a wide range of irreversible oxidative damage in the mitochondria. This in turn can lead to alterations in mitochondrial membrane potential, ATP depletion and enhanced leakage of electrons from the respiratory chain, leading to the formation of more ROS. This self-perpetuating vicious cycle may play a critical role in cell death [32]. Our results have shown irradiation of cells with 5 μM Hoechst 33342 resulted in a decrease in ΔΨm at early time points similar to the results reported earlier in HL-60 leukaemic cells treated with the lower concentration of Hoechst 33342 [10] but did not lead to cell death (Figure 7A). This suggests that a transient increase in ROS at early time due to irradiation leading to a decrease in mitochondrial membrane potential was insufficient to induce death of the cell; rather irradiation of cells in the presence of Hoechst 33342 at later time due to continuous accumulation of ROS resulted in an increase in ΔΨm which might contribute to increased cell death. Both confocal images and flow cytometric evaluation using JC-1 and rhodamine 123 fluorescent dyes, respectively, have shown a clear correlation between the increase in ROS generation and increased ΔΨm at later time points when cells were irradiated with Hoechst 33342 (Figures 2B and 7B). These results are similar to an earlier report that described the close relationship between the increases in ROS with increased ΔΨm with proteasome inhibitor, bortezomib treated human H460 lung cancer cells [33]. In addition an increase in mitochondria number due to increase in ROS in human cells was also reported [20]. Similarly, our results show that irradiation of cells with Hoechst 33342 enhanced biogenesis of mitochondria observed by labelling the cell with mitochondrial specific dye (NAO) which bind with the cardiolipin in mitochondrial membrane due to large accumulation of ROS (data not shown).

Increased ROS leading to growth delay and cell cycle perturbations are emphatically described in the literature [34]. In this study, Hoechst 33342 in combination with radiation significantly inhibited the growth of BMG-1 cells. It is widely accepted that activation of checkpoint in response to DNA damage leads to cell cycle arrest and depending upon the extent of damage can lead to apoptotic cell death. G_2/M check point is a very important restriction point before mitosis in eukaryotic cells. G_2/M arrest provides an essential period for DNA repair before the segregation of chromosome, prevents the failure in mitosis and increases the tolerance to DNA damaging agents such as some chemotherapeutic compounds and ionizing radiation. Ionizing radiation-induced cell cycle perturbations and G_2/M block observed in different cell lines [35] have been implicated for radiation-induced cell death. The cell death will depend on the nature of perturbations caused by the combined effect of radiation and Hoechst. Estimation of the distribution of cells in different phases of cell cycle can provide an insight on this combined treatment. The observed increase in G_2/M fractions (46%) as compared to radiation alone (23%) at 48 h after the treatment, which remained arrested up to 72 h, has contributed to radiosensitization by Hoechst 33342. Consequences of such an extended delay in G_2/M were expected for induction of death processes. Sulforaphane has shown similar effects, where induction of G_2/M arrest was attributed to ROS-mediated activation of ATM/Chk2 leading to Ser-216 phosphorylation and cytoplasmic sequestration of Cdc25C [36].

Necrosis and apoptosis are the two major death processes induced by a variety of cytotoxic agents that contributes to loss of clonogenicity, while mitotic death is a major contributor following ionizing radiation [37]. A lack of correlation between the induction of apoptosis and loss of clonogenicity (cell survival) has been demonstrated in a variety of cell lines following irradiation, suggesting other death processes (such as mitotic death). The role of ROS contributing to the gamma radiation-induced formation of micronuclei has also been suggested [38]. The present results suggest that the combination of Hoechst 33342 and radiation could facilitate radiation-induced cell death through multiple pathways. A proportionate increase (34%) in micronuclei formation observed in this study suggests that enhanced mitotic death is partly responsible for the cell death. Further, mitotic death, one of the primary effects responsible for the loss of clonogenicity in most of the epithelial tumours, is also often followed by delayed apoptosis as a secondary event [39,40]. Increase in the fraction of annexin V positive cells following irradiation observed in the presence of Hoechst 33342 indicated apoptotic cell death as well. Irradiation of cells with Hoechst 33342 led to both apoptotic and necrotic modes of cell death, which were also represented by DIC images of cells (Figure 6B and C). Therefore, under these conditions, it appears that both mitotic and apoptotic death are enhanced, thereby leading to a higher level of cell kill.

Increase in the activity and expression of cellular antioxidant enzymes in response to ROS is a well known adaptive phenomena for reducing cytotoxicity [41–43]. Our results also showed that Hoechst 33342 significantly increased the activity and level of Mn-SOD, which is essentially located in the mitochondria and acts as a first line of defense against oxidative insult at mitochondria. However, there was marginal change in the activity and level of catalase observed. These results indicated the accumulation of hydrogen peroxide in mitochondria for a longer

duration due to increased expression of Mn-SOD which dismutate the superoxide to hydrogen peroxide. Therefore, non-coordinated expression of Mn-SOD and catalase due to the treatment resulted in enhanced cell death. Earlier and similar recent observations at our lab have shown that no simultaneous up-regulation of Mn-SOD and catalase in p53-dependent cell resulted in enhanced oxidative stress [44,45].

Conclusion

Hoechst 33342, the DNA minor groove binder, has the ability to bind with mitochondrial DNA and induces mitochondrial dysfunction by apparently altering the electron transfer through complex I of the ETC chain, resulting in accumulation of ROS which in turn alters the mitochondrial membrane potential leading to death via multiple modes. This understanding is expected to benefit both in elucidating the detailed mechanisms of actions of DNA interacting drug in internal milieu of cell and designing better molecules for enhancing radiation-induced cell kill for cancer treatment. Further studies on the generality of these observations in other cells and the effect of Hoechst 33342 on the expression of sub-units of ETC encoded by mtDNA are in progress.

Acknowledgement

We are thankful to Dr R. P. Tripathi, Director, Institute of Nuclear Medicine and Allied Sciences for support and constant encouragement.

Declaration of interest: This work was carried out as part of a project (INM 301) supported by DRDO from the Ministry of Defense, Government of India. Mr Mohammad Athar is a recipient of ICMR fellowship. The authors report no conflicts of interest. The authors alone are responsible for the content and writing of the paper.

References

[1] Chen AY, Yu C, Bodley A, Peng LF, Liu LF. A new mammalian DNA topoisomerase I poison Hoechst 33342: cytotoxicity and drug resistance in human cell cultures. Cancer Res 1993;53:1332–1337.

[2] Chen AY, Yu C, Gatto B, Liu LF. DNA minor groove-binding ligands: a different class of mammalian DNA topoisomerase I inhibitors. Proc Natl Acad Sci USA 1993;90:8131–8135.

[3] Kiechle FL, Zhang X. Hoechst 33342 induces apoptosis and alters TATA box binding protein/DNA complexes in nuclei from HL-60 cells. J Clin Ligand Assay 1998;21:413–417.

[4] Zhang X, Kiechle FL. Hoechst 33342–induced apoptosis is associated with intracellular accumulation of E2F-1 Protein in BC3H-1 myocytes and HL-60 cells. Arch Path Lab Med 2001;125:99–104.

[5] Adhikari JS, Khaitan D, Arya MB, Dwarakanath BS. Heterogeneity in the radiosensitizing effects of the DNA ligand hoechst-33342 in human tumor cell lines. J Cancer Res Ther 2005;1:151–161.

[6] Tawar U, Jain AK, Chandra R, Singh Y, Dwarakanath BS, Chaudhury NK, Good L, Tandon V. Minor groove binding DNA ligands with expanded A/T sequence length recognition, selective binding to bent DNA regions and enhanced fluorescent properties. Biochemistry 2003;42:13339–13346.

[7] Ren J, Chaires JB. Sequence and structural selectivity of nucleic acid binding ligands. Biochemistry 1999;38: 16067–16075.

[8] Haq I, Ladbury JE, Chowdhry BZ, Jenkins TC, Chaires JB. Specific binding of Hoechst 33258 to the d (CGCAAATTT GCG) 2 duplex: calorimetric and spectroscopic studies. J Mol Biol 1997;271:244–257.

[9] Singh KK, Russell J, Sigala B, Zhang Y, Williams J, Keshav KF. Mitochondrial DNA determines the cellular response to cancer therapeutic agents. Oncogene 1999;18:6641–6646.

[10] Chen JC, Zhang X, Singleton TP, Kiechle FL. Mitochondrial membrane potential change induced by Hoechst 33342 in myelogenous leukemia cell line HL-60. Ann Clin Lab Sci 2004; 34:458–466.

[11] Zhang X, Kiechle FL. Fatty acid synthase and its mRNA concentrations are decreased at different times following Hoechst 33342-induced apoptosis in BC3H-1 myocytes. Ann Clin Lab Sci 2006;36:185–193.

[12] Mattson DM, Ahmad IM, Dayal D, Parsons AD, Aykin-Burns N, Li L, Orcutt KP, Spitz DR, Dornfeld KJ, Simons AL. Cisplatin combined with zidovudine enhances cytotoxicity and oxidative stress in human head and neck cancer cells via a thiol-dependent mechanism. Free Radic Biol Med 2009; 46:232–237.

[13] Dwarkanath BS, Jain VK. Energy linked modifications of the radiation response in a human cerebral glioma cell line. Int J Radiat Oncol Biol Phys 1989;17:1033–1040.

[14] Tamura K, Aotsuka T. Rapid isolation method of animal mitochondrial DNA by the alkaline lysis procedure. Biochem Genet 1988;26:815–819.

[15] Chaudhury NK, Bhardwaj R. Structural stabilization by Hoechst 333258 in γ-irradiated DNA: evidenced by spectroscopic studies. Curr Sci 2004;87:1256–1262.

[16] Rothe G, Valet G. Flow cytometric analysis of respiratory burst activity in phagocytes with hydroethidine and 2', 7'-dichlorofluorescin. J Leukocyte Biol 1990;47:440–448.

[17] Narayanan PK, Goodwin EH, Lehnert BE. Alpha particles initiate biological production of superoxide anions and hydrogen peroxide in human cells. Cancer Res 1997;57:3963–3971.

[18] Zölzer F, Hillebrandt S, Streffer C. Radiation induced G1-block and p53 status in six human cell lines. Radioth Oncol 1995;37:20–28.

[19] Vermes I, Haanen C, Steffens-Nakken H, Reutellingsperger C. A novel assay for apoptosis flow cytometric detection of phosphatidylserine expression on early apoptotic cells using fluorescein labelled annexin V. J Immunol Methods 1995; 184:39–51.

[20] Lee HC, Yin PH, Lu CY, Chi CW, Wei YH. Increase of mitochondria and mitochondrial DNA in response to oxidative stress in human cells. Biochem J 2000;348:425–432.

[21] Maftah A, Ratinaud M, Dumas M, Bonte F, Meybeck A, Julien R. Human epidermal cells progressively lose their cardiolipins during ageing without change in mitochondrial transmembrane potential. Mech Ageing Dev 1994;77:83–96.

[22] Harshman KD, Dervan PB. Molecular recognition of B-DNA by Hoechst 33258. Nucleic Acids Res 1985;13:4825–4835.

[23] Andrews RM, Kubacka I, Chinnery PF, Lightowlers RN, Turnbull DM, Howell N. Reanalysis and revision of the cambridge reference sequence for human mitochondrial DNA. Nat Genet 1999;23:147.

[24] Varshney R, Dwarakanath BS, Jain V. Radiosensitization by 6-aminonicotinamide and 2-deoxy-D-glucose in human cancer cells. Int J Radiat Biol 2005;81:397–408.
[25] Cosa G, Focsaneanu KS, McLean JR, McNamee JP, Scaiano JC. Photophysical properties of fluorescent DNA-dyes bound to single-and double-stranded DNA in aqueous buffered solution. Photochem Photobiol 2001;73:585–599.
[26] Jin R, Breslauer KJ. Characterization of the minor groove environment in a drug-DNA complex: bisbenzimide bound to the poly [d (AT)]. poly [d (AT)] duplex. Proc Natl Acad Sci USA 1988;85:8939–8942.
[27] Latt SA, Wohlleb JC. Optical studies of the interaction of 33258 Hoechst with DNA, chromatin, and metaphase chromosomes. Chromosoma 1975;52:297–316.
[28] Maiti S, Chaudhury NK, Chowdhury S. Hoechst 33258 binds to G-quadruplex in the promoter region of human c-myc. Biochem Biophys Res Commun 2003;310:505–512.
[29] Adhikary A, Buschmann V, Muller C, Sauer M. Ensemble and single-molecule fluorescence spectroscopic study of the binding modes of the bis-benzimidazole derivative Hoechst 33258 with DNA. Nucleic Acids Res 2003;31:2178–2186.
[30] Balaban RS, Nemoto S, Finkel T. Mitochondria, oxidants, and aging. Cell 2005;120:483–495.
[31] Singh SV, Srivastava SK, Choi S, Lew KL, Antosiewicz J, Xiao D, Zeng Y, Watkins SC, Johnson CS, Trump DL, Lee YJ, Xiao H, Herman-Antosiewicz A. Sulforaphane-induced cell death in human prostate cancer cells is initiated by reactive oxygen species. J Biol Chem 2005;280:19911–19924.
[32] Kim GJ, Chandrasekaran K, Morgan WF. Mitochondrial dysfunction, persistently elevated levels of reactive oxygen species and radiation-induced genomic instability: a review. Mutagenesis 2006;21:361–367.
[33] Ling YH, Liebes L, Zou Y, Perez-Soler R. Reactive oxygen species generation and mitochondrial dysfunction in the apoptotic response to Bortezomib, a novel proteasome inhibitor, in human H460 non-small cell lung cancer cells. J Biol Chem 2003;278:33714–33723.
[34] Burdon RH. Superoxide and hydrogen peroxide in relation to mammalian cell proliferation. Free Radic Biol Med 1995;18:775–794.
[35] Hwang A, Muschel RJ. Radiation and the G 2 phase of the cell cycle. Radiat Res 1998;150:S52–S59.

This paper was first published online on Early Online on 17 June 2010.

[36] Singh SV, Herman-Antosiewicz A, Singh AV, Lew KL, Srivastava SK, Kamath R, Brown KD, Zhang L, Baskaran R. Sulforaphane-induced G2/M phase cell cycle arrest involves checkpoint kinase 2-mediated phosphorylation of cell division cycle 25C. J Biol Chem 2004;279:25813–25822.
[37] Hendry JH, West CM. Apoptosis and mitotic cell death: their relative contributions to normal-tissue and tumour radiation response. Int J Radiat Biol 1997;71:709–719.
[38] Akudugu JM, Bohm L. Micronuclei and apoptosis in glioma and neuroblastoma cell lines and role of other lesions in the reconstruction of cellular radiosensitivity. Radiat Environ Biophys 2001;40:295–300.
[39] Meyn RE, Stephens LC, Ang KK, Hunter NR, Brock WA, Milas L, Peters LJ. Heterogeneity in the development of apoptosis in irradiated murine tumours of different histologies. Int J Radiat Biol 1993;64:583–591.
[40] Held KD. Radiation-induced apoptosis and its relationship to loss of clonogenic survival. Apoptosis 1997;2:265–282.
[41] Guo G, Yan-Sanders Y, Lyn-Cook BD, Wang T, Tamae D, Ogi J, Khaletskiy A, Li Z, Weydert C, Longmate JA, Huang TT, Spitz DR, Oberley LW, Li JJ. Manganese superoxide dismutase-mediated gene expression in radiation-induced adaptive responses. Mol Cell Biol 2003;23:2362–2378.
[42] Summers RW, Maves BV, Reeves RD, Arjes LJ, Oberley LW. Irradiation increases superoxide dismutase in rat intestinal smooth muscle. Free Radic Biol Med 1989;6:261–270.
[43] Oberley LW, St Clair DK, Autor AP, Oberley TD. Increase in manganese superoxide dismutase activity in the mouse heart after X-irradiation. Arch Biochem Biophys 1987;254:69–80.
[44] Hussain SP, Amstad P, He P, Robles A, Lupold S, Kaneko I, Ichimiya M, Sengupta S, Mechanic L, Okamura S, Hofseth LJ, Moake M, Nagashima M, Forrester KS, Harris CC. p53-induced up-regulation of MnSOD and GPx but not catalase increases oxidative stress and apoptosis. Cancer Res 2004;64:2350–2356.
[45] Sharma PK, Bhardwaj R, Dwarakanath BS, Varshney R. Metabolic oxidative stress induced by a combination of 2-DG and 6-AN enhances radiation damage selectively in malignant cells via non-coordinated expression of antioxidant enzymes. Cancer Lett (In Press).